Northumbria Research Link

Citation: Ait Si Ali, Amine, Farhat, Ali, Mohamad, Saqib, Amira, Abbes, Bensaali, Faycal, Benammar, Mohieddine and Bermak, Amine (2018) Embedded Platform for Gas Applications Using Hardware/Software Co-Design and RFID. IEEE Sensors Journal, 18 (11). pp. 4633-4642. ISSN 1530-437X

Published by: IEEE

URL: https://doi.org/10.1109/JSEN.2018.2822711 <https://doi.org/10.1109/JSEN.2018.2822711>

This version was downloaded from Northumbria Research Link: http://nrl.northumbria.ac.uk/id/eprint/33914/

Northumbria University has developed Northumbria Research Link (NRL) to enable users to access the University's research output. Copyright © and moral rights for items on NRL are retained by the individual author(s) and/or other copyright owners. Single copies of full items can be reproduced, displayed or performed, and given to third parties in any format or medium for personal research or study, educational, or not-for-profit purposes without prior permission or charge, provided the authors, title and full bibliographic details are given, as well as a hyperlink and/or URL to the original metadata page. The content must not be changed in any way. Full items must not be sold commercially in any format or medium without formal permission of the copyright holder. The full policy is available online: http://nrl.northumbria.ac.uk/policies.html

This document may differ from the final, published version of the research and has been made available online in accordance with publisher policies. To read and/or cite from the published version of the research, please visit the publisher's website (a subscription may be required.)

Northumbria University NEWCASTLE

University Library

# Embedded Platform for Gas Applications Using Hardware/Software Co-Design and RFID

Amine Ait Si Ali, Ali Farhat, *Student Member, IEEE,* Saqib Mohamad, Abbes Amira, *Senior Member, IEEE,* Faycal Bensaali, *Senior Member, IEEE,* Mohieddine Benammar, *Senior Member, IEEE,* and Amine Bermak, *Fellow, IEEE,*

***Abstract*—This paper presents the development of a wireless low power reconfigurable self-calibrated multi-sensing platform for gas sensing applications. The proposed electronic nose (EN) system monitors gas temperatures, concentrations and mixtures wirelessly using the radio-frequency identification (RFID) technology. The EN takes the form of a set of gas and temperature sensors as well as multiple pattern recognition algorithms implemented on the Zynq system on chip (SoC) platform. The gas and temperature sensors are integrated on a semi-passive RFID tag to reduce the consumed power. Various gas sensors are tested including an in-house fabricated $4 \times 4$ $SnO_2$ based sensor and 7 commercial Figaro sensors. The Data is transmitted to the Zynq based processing unit using a RFID reader where it is processed using multiple pattern recognition algorithms for dimensionality reduction and classification. Multiple algorithms are explored for optimum performance including principal component analysis (PCA) and linear discriminant analysis (LDA) for dimensionality reduction while decision tree (DT) and k-nearest neighbors (KNN) are assessed for classification purpose. Different gases are targeted at diverse concentration including carbon monoxide ($CO$), ethanol ($C_2H_6O$), carbon dioxide ($CO_2$), propane ($C_3H_8$), ammonia ($NH_3$) and hydrogen ($H_2$). An accuracy of 100% is achieved in many cases with an overall accuracy above 90% in most scenarios. Finally, the hardware/software heterogeneous solution to implementation PCA, LDA, DT and KNN on the Zynq SoC shows promising results in terms of resources usage, power consumption and processing time.**

***Index Terms*—RFID Tag, Zynq SoC, E-Nose, Real-time Processing, Gas Sensing, Temperature Sensing.**

## I. Introduction

THE integration of sensors with wireless communication technologies has recently gained a lot of interest among various areas such as monitoring, security and logistics [1]–[4]. Wireless sensing systems are usually powered by limited or even no energy sources due to cost and maintenance considerations. Thus, integrating sensors with the radio-frequency identification (RFID) technology concentrates mainly on minimizing the power consumption leading to the concept of Sensor Tag [3]–[6]. The sensor tag is an RFID tag that has sensing capabilities to monitor physical parameters while supporting the same identification function of a normal RFID tag [6], [7]. Both passive and semi-passive RFID tags are being integrated due to their low power consumption where the tag consumes an electric current as low as a few microamperes [1], [3], [4], [8]. Actually, the passive RFID tags harvest the energy from the RF signal of the RFID reader through rectifying the incoming RF signal. Most sensor tags reported in the literature has very basic sensing capabilities, such as temperature, and are typically power-hungry. This is mainly the case because the sensor tag technology is a very challenging concept not only at the integration level but also in terms of specifications [3].

Indeed, integrating sensors with RFID requires meeting very challenging specifications and constraints. Firstly, the sensors need to operate at extremely low power to avoid affecting the tag lifetime or limiting its coverage range. For instance, reported power consumption of temperature sensors for RFID applications is around tens to hundreds microwatts, which does not suite RFID applications [5], [7]. However, gas sensors power demand increases to reach a few hundred milliwatts making the integration of gas sensors on RFID tags extremely challenging [9]. This increase is due to the requirement of heating a sensing film at high temperatures [9]. Secondly, the sensors deployed in RFID devices require minimal or preferably no human intervention such as battery replacement or sensors calibration. For instance, temperature sensors often require gain and offset calibration [10]. Chemical and gas sensors typically suffer from drift issues and sensor poisoning, which is a gain and offset shift of the sensors response after exposure to target species [11], [12]. Current commercially available electronic nose (EN) systems require frequent supervised calibration (sometimes on a daily basis). This would be prohibitively expensive for RFID applications involving a very large number of deployed sensors. In addition, current chemical and gas sensors have limited sensitivity, an inability to deal with non-stationary background odors and are unable to discriminate between odor quality and odor concentration. These power and calibration issues are real obstacles that need to be addressed before the birth of sensor tags and their deployment in large scale RFID applications can truly be witnessed. A new generation of temperature and gas sensors is therefore required in order to meet the future demand of a low cost, reliable, real-time, portable and self-calibrated multi-sensing platform.

A. Ait Si Ali is with Faculty of Engineering and Environment, University of Northumbria, Newcastle, United Kingdom (e-mail: amine.ali@northumbria.ac.uk).

A. Farhat is with Department of Electrical Engineering and KINDI Center for Computing Research, Qatar University, Doha, Qatar.

S. Mohamad is with Department of ECE, Hong Kong University of Science and Technology, Hong Kong.

A. Amira is with Department of Computer Science and Engineering, Qatar University, Doha, Qatar.

F. Bensaali and M. Benammar are with Department of Electrical Engineering, Qatar University, Doha, Qatar.

A. Bermak is with College of Science and Engineering, Hamad Bin Khalifa University, Doha, Qatar.

In this paper, a new generation of ultra-low power and self-calibrated multi-sensing platform for RFID applications is proposed and developed. The platform mainly focuses on temperature and gas measurements that could be used in several applications including gas processing, security and logistics and shipment industries. The applications of this multi-sensing platform can also be extended to include environmental monitoring and pollution control, which are important applications globally. The objectives are: Firstly, develop an innovative temperature sensor featuring compactness, ultra-low power consumption and improved calibration capabilities. Secondly, develop an innovative tin-oxide gas sensor featuring CMOS compatibility, low power consumption and time-domain sensor calibration using logarithmic read-out and ADC-free technology. Thirdly, integrate both temperature and gas sensors into a semi-passive RFID tag. Finally, develop a reconfigurable SoC platform for real-time data processing, fusion, analysis and classification to replace the used PC as shown later. The remaining part of the paper is organized as follows: Section 2 is concerned with the literature review related to sensors integration in an RFID tag as well as data processing and gas identification. An overview of the proposed system is presented in Section 3. Section 4 describes the implementation of the system as well as the results, where Section 5 concludes the paper.

## II. Related work

Many researchers have already tried to integrate sensors in an RFID tag such as in [13] where a carbon nanotube based gas sensor is integrated into a passive and low cost RFID tag. The sensor has been successfully tested to detect $NH_3$ gas. However, considerable optimization and improvement is to be done. Another similar work where a gas sensor based on carbon nanotube is integrated into an RFID tag has been presented in [14] and used for the detection of small quantities of toxic gases like nitrogen oxide or ammonia. A temperature sensor have been integrated into a passive RFID tag in [15], the tag is tested and it achieves real-time wireless communication with RFID readers and the operating temperature is between $-20\,^{\circ}\mathrm{C}$ and $30\,^{\circ}\mathrm{C}$.

Many hardware based EN can be found in the literature. In [16], a committee machine gas identification system and its implementation on field programmable gate arrays (FPGA) is presented. The major contribution is that the gas identification system combines between five different classifiers to increase the accuracy. The used classifiers include multilayer perceptron (MLP), Gaussian mixture model (GMM), radial basis function (RBF), k-nearest neighbors (KNN) and probabilistic principal component analysis (PPCA). Prior to the classification process, data is normalized using euclidean normalization to set a range of values for all sensors and principal component analysis (PCA) is applied to reduce the dimensionality of the output. It is worth mentioning that the highest accuracy of $95\%$ is obtained when using the committee machine along with 8 PCAs while individual classifiers accuracies are ranging between $79.1\%$ and $92.3\%$. The gas identification system presented in [16] is also implemented on an FPGA. An MLP based identification system and its implementation on FPGA is presented in [17]. Similarly to [16], an array of eight micro-hotplate-based $SnO_2$ thin film gas sensors is used in the EN to solve problems related to the non-selectivity issue and euclidean normalization is used. However, the difference is that MLP is used as a classifier achieving an accuracy of $93.75\%$ while using five neurons as output and eight as input to match the five different gases and eight gas sensors respectively.

Another hardware implementation of an EN is presented in [18] and [19]. The innovation in this work is that a logarithmic spike timing encoding scheme is used at the pre-processing stage to create a unique signature for each gas independently of its concentration. The logarithmic spike timing encoding technique allows the conversion of signals generated by an array of 16 sensors to successive 16 spikes, each spike corresponds to a given sensor and will appear at a specific time. The order and the time of appearance of spikes is unique to each gas. The fact that the spike train (set of spikes) is unique to each gas, a simple rank order technique can be used to perform the classification. It is worth mentioning that a classification accuracy of $88.6\%$ is achieved with this technique. The work presented in [20] is another example of a pure hardware implementation of an EN on FPGA. The EN uses decision tree (DT) as a classifier, linear (Axis-Parallel) and non-linear (oblique) DT are evaluated. Performances are estimated with and without PCA as a dimensionality reduction technique. Results have shown that the best performances are obtained when using four PCAs reaching an accuracy of $99.55\%$ when using a linear DT and $94.55\%$ when a non-linear DT is used. It is worth mentioning that the only EN implemented on hardware is the one based on linear DT and without dimensionality reduction due to its simplicity.

Various software based EN can be found in the literature. [21] presents a software based EN implementation. It is based on the same type of gas sensors compared to [16] and [17]. However, it has double the number of sensors, which is 16. The innovation in this work is related to the way data is collected. In fact, data is generated by heating sensors multiple times and generating responses at various temperatures. The use of temperature modulation increased the number of 16 physical sensor to 12000 virtual ones. The self organized maps technique is used to combine the 12000 virtual sensor's responses into a 2D image which will be representing the gas signature. Image moments are then extracted from images and used as features representing a given gas at a specific concentration. Those features are used for classification. In addition, dimensionality reduction is applied before classification using linear discriminant analysis (LDA). Finally, PPCA, MLP, KNN, RBF, and GMM are individually assessed as classifiers. The best accuracy which is $96.2\%$ is reached when using GMM.

A system to monitor odors is presented in [22]. The system uses eight $SnO_2$ based sensors. The development of the neural-genetic classification algorithm which is the combination between artificial neural network and genetic algorithm represents the innovation in this work. In addition, sensors' responses are normalized to a 0-1 range. Noisy parts

in raw signals are removed by using smoothed moving average before the classification step. An accuracy of $95\%$ is achieved while it reaches only $91\%$ for genetic algorithm and $82\%$ for artificial neural network when used separately. Classifiers based on discriminant functions and density models are compared and suitability for gas identification assessed in [23]. The density models are represented by generative topographic mapping, GMM and KNN. The discriminant functions one are represented by generalized linear model, MLP and RBF. In addition, neuroscale, LDA and PCA are also assessed to perform preprocessing and dimensionality reduction. The best results are obtained when combining PCA and GMM with a reported $92.7\%$ accuracy.

In contrast to the work presented in [18] and [19], the same authors developed in [24] an improved EN that does not use the steady states as features. The proposed system use exponential moving average to extract transient features which are used for classification. The major advantage in using the transient features over steady states is that those features are obtained much earlier than the steady states which will speed up the classification process even if this results in using a vector of feature instead of a single value. Furthermore, the system uses Bayesian inference along with random matrix theory for classification purpose. An accuracy of $99.40\%$ is achieved with this method.

Probabilistic rank score coding is used in [25] to implement an improved EN which uses rank orders. In the rank order based technique, the gas signature is represented by temporal spikes. The disadvantage of using spikes to identify gases is that the variation in sensors' responses when exposed to same gas at the same concentration will result in temporal variation in the spiking sequences. Therefore, performances will decrease. Probabilistic rank score coding helps solving this issue by generating a probability at each rank in a tabular form. The classification stage takes into consideration those probabilities. Two set of sensors are used to evaluate the performances of this approach. It has been shown that a $100\%$ accuracy has been achieved in both scenarios. [26] is another work where the same probability rank tables are used . Cluster-k-nearest neighbors (CKNN) and tree-CKNN are two improved classification algorithms based on KNN and presented in [27]. It has been claimed that both CKNN and tree-CKNN perform better that KNN by reaching an accuracy of $98.7\%$ for CKNN and $100\%$ respectively without applying dimensionality reduction techniques as preprocessing step. Another DT based EN is presented in [28]. Five gases are targeted in this work and seven sensors are used.

## III. Proposed system overview

The overview of the proposed multi-sensing reconfigurable low power and self-calibrated platform for efficient gas monitoring can be seen in figure 1. The platform is made of two main parts: (1) the developed RFID sensing system using the SL900A RFID tag that will store sensors' readings and (2) the proposed gas identification data processing unit, which is a PC that runs Microsoft Visual Studio and MATLAB or the Xilinx Zynq SoC for hardware acceleration. In between those two parts, there are few commercially available items including a ThingMagic M6e RFID reader and its antenna as well as a mouse, a keyboard and a monitor to display the output of the Xilinx SoC. The Arduino UNO microcontroller collects temperature and gas data from the sensors to store them on the SL900A RFID tag. Subsequently, the processing units gets the stored data from the tag using the RFID reader and the antenna. Using pattern recognition algorithms such as PCA, LDA, DT and KNN that are either running on MATLAB or implemented on the Zynq SoC based prototyping board (ZC702) to process the data as fast as possible and perform gas classification in real-time. For both processing units, the acquired results are visualized on the monitor. It is worth noting that the Microsoft Visual Studio is used to program the ThingMagic M6e RFID reader as it is not compatible with MATLAB.

TABLE I
Sensors specifications

| Sensors | Target Gases | Concentration (ppm) | Power (mW) |
|---|---|---|---|
| TGS826 | $NH_3$ | 30-300 | 833 |
| TGS2442 | CO | 30-1000 | 14 |
| TGS2600 | $H_2$ | 1-30 | 210 |
| TGS2602 | $C_2H_6O$ | 1-30 | 280 |
| TGS2610 | $C_4H_{10}$ & C3H8 | 500-10000 | 280 |
| TGS2611 | CH4 | 500-10000 | 280 |
| TGS2620 | Alcohol & Solvent vapors | 50-5000 | 210 |
| In-house 4x4 | $CO$<br>$H_2$<br>$C_2H_6O$<br>$CH_4$ | 25-260<br>25-800<br>50-200<br>500-5000 | 352 |

## IV. System implementation and results

### A. RFID TAG

*1) Gas sensor:* It has been decided to use an array of sensors over a single sensor to overcome the non-selectivity problem and for better performances in terms of gas discrimination. Two sets of gas sensors are tested and evaluated, one using a set of seven Figaro sensors [29] and the second one using an array of $4by4$ fabricated sensors [30]. Sensors specifications in terms of target gases, typical concentration detection range and power consumption are listed in table I.

The mention TGS refer to the commercial Figaro sensors used to form the sensor array. The layout of the $4 \times 4$ sensor is made of 16 sections organized in four rows and four columns where each section represents one sensor. To modify the response of the $SnO_2$ sensing film for each part, a post treatment is performed during the fabrication process to improve the selectivity by depositing various noble metal additives on the sensing film. The post treatment is realized by metal doping and ion implantation during the fabrication process. Therefore, all presented results and performances are related to the post treatment scheme. Three noble metals (Platinum ($Pt$), Palladium ($Pd$) and Gold ($Au$)) are combined with three ions (Boron ($B$), Phosphorus ($P$) and Hydrogen ($H$)). A summary of the post treatment is shown in table II. It is worth mentioning the sensors use microhotplates

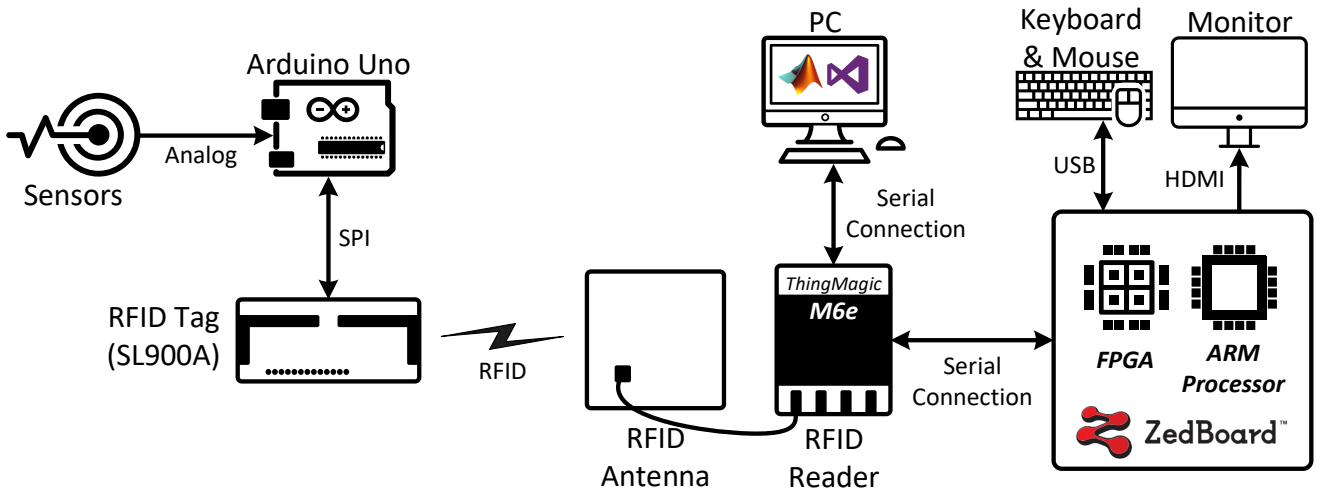


Fig. 1. Overview of the multi-sensing platform

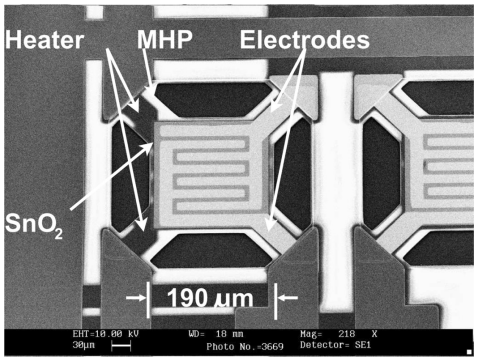


Fig. 2. Scanning electron microscopy picture of the fabricated gas sensor element [30]

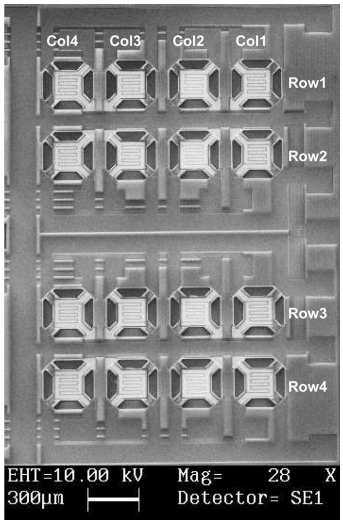


Fig. 3. Scanning electron microscopy picture of the fabricated $4 \times 4$ gas sensor array [30]

TABLE II
$4 \times 4$ SENSOR ARRAY POST TREATMENT SCHEME

| Row | Column 1 | Column 2 | Column 3 | Column 4 |
|---|---|---|---|---|
| 1 | N/A | $Pt$ | $Pd$ | $Au$ |
| 2 | $B$ | $Pt/B$ | $Pd/B$ | $Au/B$ |
| 3 | $P$ | $Pt/P$ | $Pd/P$ | $Au/P$ |
| 4 | $H$ | $Pt/H$ | $Pd/H$ | $Au/H$ |

structures to increase the operating temperature, the cross-sectional scanning electron microscopy picture of the MHP structure is shown in figure 2, while the scanning electron microscopy picture of the fabricated sensor element is shown in figure 3.

*2) Temperature sensor:* A time to digital based digital converter with a sub micro-watt power consumption, which makes it suitable for sensing applications in low power environments like RFID tags is presented here. A temperature independent current is also generated in the front end and then used to bias a voltage-to-time converter cell which generates a temperature modulated output pulse. This pulse can then be digitized with an external clock to obtain an estimate of the temperature.

Figure 4 shows the circuit diagram of the temperature sensor. The proportional to absolute temperature (PTAT) and complementary to absolute temperature (CTAT) voltages ($V_{PTAT}$ and $V_{CTAT}$) are generated in a bipolar junction transistor (BJT) based front-end (Figure 5). These voltages are converted into a pulse using the voltage-to-time converter which consists of a capacitor C, a continuous time comparator and a discharge current source ($I_{dis}$), which is implemented with a NMOS transistor biased in subthreshold. The bias current ($I_{bias}$) for the comparator is also derived from the BJT front end.

The output of the comparator is a pulse ($V_{out}$). In the sense high phase, the switch $S_1$ (implemented as a transmission gate) is closed and the voltage $V_{CTAT}$ is sampled on the capacitor C so that $V_X = V_{CTAT}$ . As soon as sense goes low, the switch $S_2$ is closed, thus discharging the top plate of the capacitor. When the capacitor voltage crosses the voltage at the negative

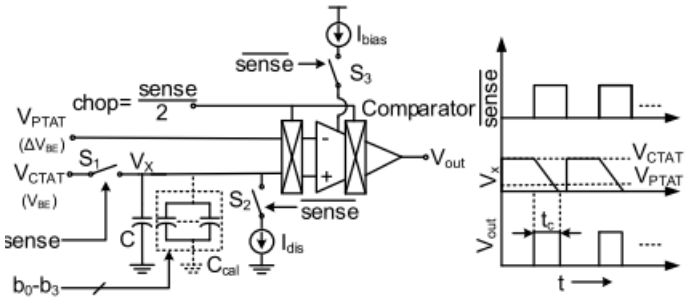


Fig. 4. The circuit diagram of the proposed temperature sensor

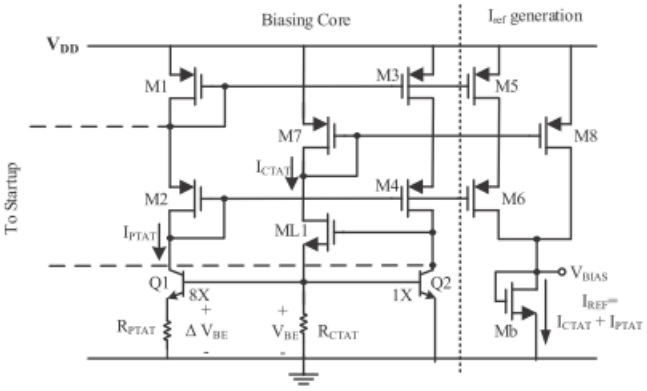


Fig. 5. BJT based front-end schematic that generates $V_{PTAT}$ and $V_{CTAT}$

input of the comparator, the output of the comparator goes low and an output pulse is produced. The time period $t_C$ can be written as in equation 1 (assuming an ideal comparator).

$$t_c = \frac{C(V_{PTAT} - V_{CTAT})}{I_{dis}} \tag{1}$$

It can be seen that if the discharge current is independent of temperature, the pulse width, $t_c$ decreases linearly with temperature, as long as the PTAT and CTAT voltages are linear functions of temperature. In order to conserve power during the sense phase when the voltage is being sampled on the capacitor, the comparator is turned off. This is facilitated by implementing the comparator as a switched opamp topology

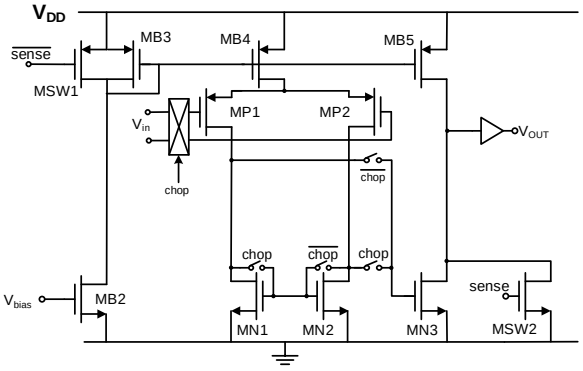


Fig. 6. Switched opamp based comparator, incorporating chopping.

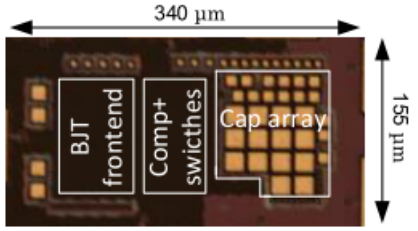


Fig. 7. Chip Micro-photograph

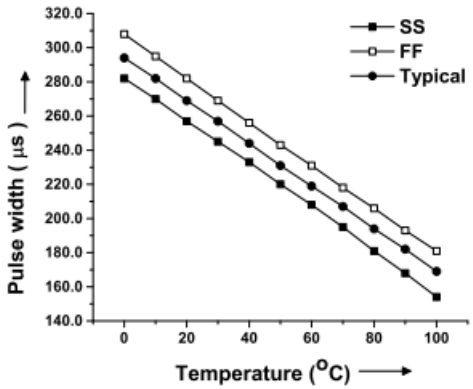


Fig. 8. Output pulse width of the temperature sensor.

(Figure 6). The supply current is switched off by means of the *MNSW1* transistor, which is controlled by the *sense* signal. Offset is also a major issue in temperature sensors, since it can introduce additional dependence of delay on temperature. The effects of the comparator offset are alleviated by chopping the comparator after every sense cycle. This is achieved by the use of a chopping block at the input pair of the comparator. The diode connected transistors *MN1* and *MN2* are also chopped to maintain a high impedance node at the gate of MN3. All the chop switches are implemented using transmission gates. The chopping also serves to lower the effects of low frequency noise.

The chip was fabricated in CSM $0.18\,\mu\mathrm{m}$ process. Figure 7 shows the microphotograph of the EN. The chip measures $340\,\mu\mathrm{m} \times 155\,\mu\mathrm{m}$ $(.0527mm^2)$. A supply voltage of 1.2 V is used. The sense signal is supplied through external clock of 2 kHz bandwidth giving a sample rate of 1 kSa/s. The actual sample rate is 100 Sa/s (after averaging). Nominal power consumption is 510 nW at $27\,^{\circ}\mathrm{C}$. Figure 8 shows the simulated pulse width across the three process corners: Nominal , SS (Slow NMOS,PMOS) corner and FF (Fast NMOS, PMOS) corner, for a range of $0\,^{\circ}\mathrm{C}$ to $100\,^{\circ}\mathrm{C}$. The sensitivity of the temperature sensor is around $1.3\mu s/^{\circ}C$. Two point calibration is used for the temperature sensor at $20\,^{\circ}\mathrm{C}$ and $60\,^{\circ}\mathrm{C}$. Calibration is achieved using the $C_{cal}$ array in figure 4, which is an array of capacitors whose size can be varied by external digital signal bits $< b_0 : b_3 >$. Maximum error is $\pm 0.9\,^{\circ}\mathrm{C}$ (Figure 9).

*3) Hardware platform for semi-passive RFID with integrated sensors:* The proposed RFID design operates in a

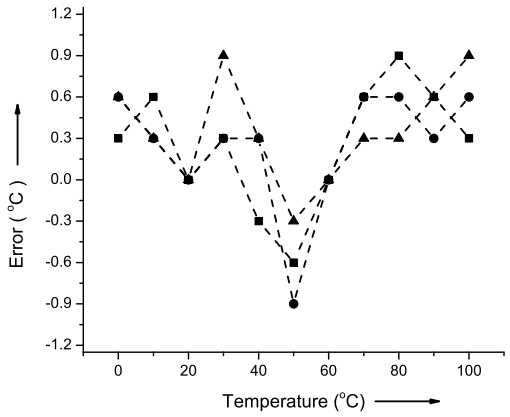


Fig. 9. Measured error across the temperature range for 3 samples.

semi-passive mode where an integrated battery or the microcontroller are used to power up the SL900A RFID tag. The SL900A RFID tag is EPC Gen2 standard compliant. The RFID tag has a 9k-bit EEPROM memory with password protection option. As shown in the figure, the design allows connecting more external sensors if needed. The proposed design is dedicated for use in smart RFID sensing platform, including semi-passive and passive tags integration. The integrated circuit (IC) includes sensor functionality and storing of sensor data. The IC is running at 860-960 MHz frequency band and is compatible with the EPC global Class 1 standard. The downlink (reader-transponder) work based on amplitude modulation where the uplink (transponder-reader) uses load shift keying modulation. The maximum tag to reader data rate based on Class 1 Gen2 standard is found to be 640 kbps and the maximum reader to tag data rate is 160 kbps [8].

In the proposed system, the RFID tag is powered using the microcontroller. The microcontroller uses the SPI serial communication interface to communicate with the RFID tag. The collected data from the sensors is written in the EEPROM's USER memory bank where each EEPROM address holds one byte of data. The size of the USER memory bank is 1051 bytes. Therefore, to store the data in the EEPROM, it should be formatted into packets of bytes where the variables are broken into several packets. Afterwards, the packets are stored in the USER memory bank. However, the RFID reader should be synchronized with the microcontroller to fetch the latest data stored to satisfy the real-time system requirement. Therefore, the first two bytes of the USER memory bank are used by the microcontroller to store the address of the latest data stored. Two bytes are required because the EEPROM has an 11-bit address that points to the physical locations of the EEPROM [8]. Subsequently, the reader reads these two bytes until their values change. When the reader detects a change in the values stored in the two bytes, the reader will jump to the identified address and read the last data stored by the microcontroller. This procedure works if and only if the RFID reader is able to read the data stored in the two bytes several times before the microcontroller updates the data. In other words, the time that takes the RFID reader to read the data from the tag is shorter than the time that takes the microcontroller to collect the data and store it in the tag. Therefore, the reader is always aware of the most recent data. Moreover, the aforementioned synchronization method is very effective especially if the data was not time stamped. It has been observed that the consumed power by the microcontroller and the RFID tag is independent from how frequently the measurements are acquired. This is due avoiding the use of the microcontroller's sleeping mode to maintain the error free RFID communication using the stated method earlier. The consumed power by the microcontroller is 304 mW while the consumed power by the RFID tag is 0.15 mW [8].

### *B. Data Processing Units*

First, the system is implemented on a PC using both Microsoft Visual Studio and MATLAB. Microsoft Visual Studio is used to program the RFID reader where the MATLAB is used to process the data fetched through the RFID reader from the RFID tag. However, the main aim of the work is to develop another processing unit using the ZC702 prototyping board [31]. The ZC702 board is based on the Zynq-7000 SoC [32]. The Zynq-7000 SoC is made of a processing system (PS) and a programmable logic (PL) in a single chip. The PS holds two ARM Cortex A9 processors and is independent from the PL. The PS also integrates external, internal memory interfaces as well as other peripherals such us USB, Ethernet, UART, CAN, I2C, SD/SDIO, SPI and GPIO. The PL is based on one of the 7 series Xilinx FPGA and in the case of the ZC702 board it is based on the Artix-7 FPGA [33]. Six different gases are targeted in total. Carbon monoxide ($CO$), Ethanol ($C_2H_6O$), Carbon dioxide ($CO_2$), Propane ($C_3H_8$), Ammonia ($NH_3$)) and Hydrogen ($H_2$). The choice of gases is for evaluation purpose, specific gases can be targeted for specific applications where the EN system can be easily adapted to handle new types of gases. It is worth mentioning that various gas data sets are collected in laboratory and used to train and test the system. The training is performed offline in MATLAB while testing and validation is performed both offline and online on the Zynq SoC platform. Various pattern recognition algorithms have been explored for the best performances including PCA and LDA for dimensionality reduction as well as DT and KNN for classification purpose as it can be seen in figure 10. In addition, the main feature extracted from the sensors outputs signals for gas identification is the steady states. It is worth mentioning that data is collected for multiple gases at different concentrations to reflect the real environment. The experimental setup is described in detail in [36]. Training, validation and testing is then performed, and results evaluated based on the entire dataset including all gases and concentrations together. Therefore, performances are not assessed separately for each concentration.

The performance of the proposed system is assessed by its accuracy. The developed system is made of two core components: the sensor tag (sensors and RFID tag), and the data processing unit (gas identification algorithms). As stated earlier, the sensor tag is responsible for acquiring the

TABLE III
EN ACCURACIES FOR $4 \times 4$ SENSOR ARRAY WHEN USING DT AND PCA

| | Classification scenarios | | | | |
|---|---|---|---|---|---|
| | Steady-states | 2-PCs | 3-PCs | 4-PCs | 5-PCs |
| Accuracy | 73.33% | 80% | 90% | 80% | 80% |

TABLE IV
EN ACCURACIES FOR 7 FIGARO SENSORS WHEN USING DT AND PCA

| | Classification scenarios | | | |
|---|---|---|---|---|
| | Steady-states | 2-PCs | 3-PCs | 4-PCs |
| Accuracy | 99% | 100% | 99% | 99% |

readings from the sensors (temperature and gas sensors) and then transmitting the data to the data processing units using the RFID technology. However, if the received data from the RFID transmission is not identical to the transmitted data, the performance of the system is affected by the RFID transmission. Therefore, the RFID transmission was tested and verified to have no errors introduced while transmitting the data (the received data is identical to the data transmitted). Subsequently, the performance of the sensors in sensing the temperature and gases and the data processing unit (algorithms) in classification are what define and limit the accuracy of the entire system. In other word, the use of the RFID tag for communication did not affect the performance of the proposed system.

The following equation 2 is used to compute the accuracy of the various implementations. Tables III to VI shows the accuracy results from MATLAB for the EN when using both sensors (In-house $4 \times 4$ and 7 Figaro) along with two different classifiers (DT and KNN) and a single dimensionality reduction technique (PCA), the choice of presenting results for PCA only came from the fact that the differences in performances between PCA and LDA are not significant. It can be seen in Table III that the best performance which is an accuracy of 90% when using DT and the $4\times4$ sensor array is obtained with the combination of the first three principal components while for the case of the Figaro sensors using the same DT classifier, the best accuracy of 100% is reached with two principal components only as shown in Table IV. A similar pattern is observed in Table V and VI when using KNN as a classifier. The best accuracy of 96.7% is reached for the $4\times4$ sensor array when using the first four principal components and just the first two principal components for the Figaro sensors with an accuracy of 100%. In both cases the best results are reached when taking in consideration the distance with the nearest neighbour only (k=1).

$$\text{Accuracy} = \frac{\text{Number of correct predictions for all gases}}{\text{Number of all testing observations}} \times 100 \quad (2)$$

All best scenarios in terms of accuracy for different algorithms have been implemented using the Zynq platform and a heterogeneous Hardware/Software design solution where

TABLE V
EN ACCURACIES FOR $4 \times 4$ SENSOR ARRAY WHEN USING KNN AND PCA

| KNN Parameters | Classification scenarios | | | | |
|---|---|---|---|---|---|
| | Steady-states | 2-PCs | 3-PCs | 4-PCs | 5-PCs |
| K=1 | 78.33% | 60% | 71.66% | 96.67% | 96.67% |
| K=2 | 73.33% | 78.33% | 80% | 81.67% | 81.67% |
| K=3 | 71.33% | 80 % | 81.67% | 81.67% | 81.67% |

TABLE VI
EN ACCURACIES FOR 7 FIGARO SENSORS WHEN USING KNN AND PCA

| KNN Parameters | Classification scenarios | | | |
|---|---|---|---|---|
| | Steady-states | 2-PCs | 3-PCs | 4-PCs |
| K=1 | 93.33 % | 100% | 100% | 100% |
| K=2 | 95.55% | 100% | 100% | 100% |
| K=3 | 95.55% | 100 % | 100% | 100% |

multiple optimization techniques have been explored when using high level synthesis [34] including array partitioning, loop unrolling and pipelining. The first Unroll directive is applied to loops and it is a very powerful directive. It allows loops to be executed in parallel having dedicated hardware resources for each loop. Array Partition is applied to the input array which results in the breakdown of the array into various sub arrays allowing multiple access in parallel. The Pipeline directive is applied to the top level function to allow pipelining of all instructions and sub functions existing inside. The last crucial AXI Lite directive helps to connect various IP-cores, especially the ones developed in Vivado HLS for a heterogeneous implementation in the PL along with the PS. Results in terms of resources usage as well as the maximum frequency and the latency can be visualised in tables VII to X. It can be seen from the tables that applying various directives helps to improve the processing time. However, more resources are used. An interactive software that uses all the mentioned algorithms have been developed in [35]. More details about the use of PCA and DT can be found in [36] while the details about the use of LDA compared to PCA can be found in [37]. Finally, the implementation of the KNN classifier have been discussed in [38].

## V. CONCLUSION

A low power reconfigurable self-calibrated multi-sensing platform for gas applications have been presented in this

TABLE VII
HARDWARE USAGE AND PERFORMANCE RESULTS FOR EN BASED ON $4 \times 4$ SENSOR ARRAY, PCA 1, 2, 3 AND DT

| Hardware resources and performance | Optimization directives | | | |
|---|---|---|---|---|
| | Without Directives | Unroll Loops | Array Partitioning and Pipelining | AXI Lite Interface |
| BRAM 18K | 0 | 0 | 0 | 8 |
| DSP48E | 15 | 15 | 136 | 68 |
| FF | 2089 | 1989 | 14730 | 9803 |
| LUT | 3925 | 4830 | 27208 | 14676 |
| Max frequency (MHz) | 142 | 142 | 142 | 142 |
| Latency (clock cycles) | 261 | 95 | 94 | 96 |

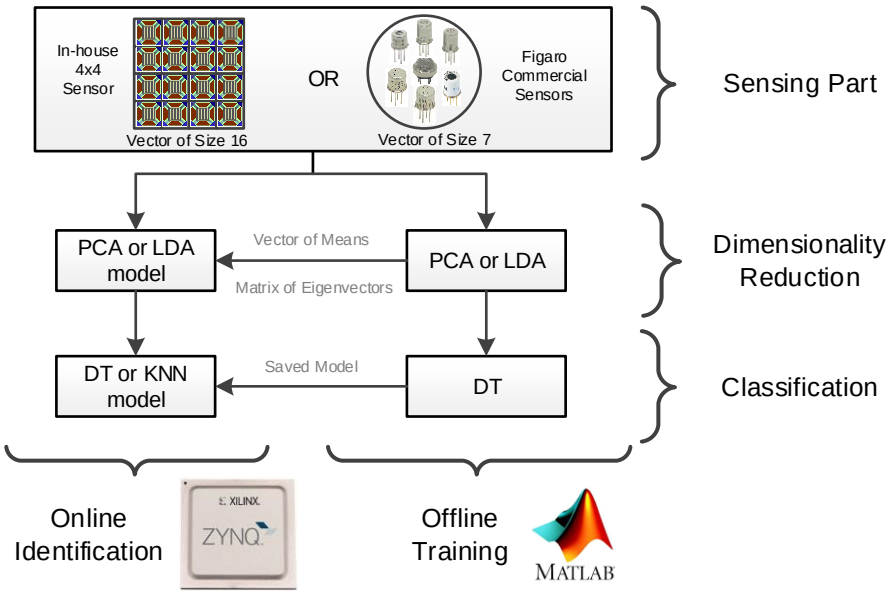


Fig. 10. EN building blocks

TABLE VIII
HARDWARE USAGE AND PERFORMANCE RESULTS FOR EN BASED ON FIGARO SENSORS, PCA 1, 2 AND DT

| Hardware resources and performance | Optimization directives | | | |
|---|---|---|---|---|
| | Without Directives | Unroll Loops | Array Partitioning and Pipelining | AXI Lite Interface |
| BRAM 18K | 0 | 0 | 0 | 0 |
| DSP48E | 10 | 10 | 84 | 84 |
| FF | 1640 | 1533 | 8387 | 8721 |
| LUT | 3042 | 3327 | 14764 | 15316 |
| Max frequency (MHz) | 142 | 142 | 142 | 142 |
| Latency (clock cycles) | 117 | 50 | 46 | 46 |

TABLE IX
HARDWARE USAGE AND PERFORMANCE RESULTS FOR EN BASED ON $4 \times 4$ SENSOR ARRAY, PCA 1, 2, 3, 4 AND KNN

| Hardware resources and performance | Optimization directives | | | |
|---|---|---|---|---|
| | Without Directives | Unroll Loops | Array Partitioning and Pipelining | AXI Lite Interface |
| BRAM 18K | 4 | 0 | 3 | 3 |
| DSP48E | 34 | 108 | 67 | 67 |
| FF | 4154 | 14524 | 8223 | 8259 |
| LUT | 6718 | 26182 | 12714 | 12754 |
| Max frequency (MHz) | 121 | 95 | 95 | 95 |
| Latency (clock cycles) | 3162 | 185 | 292 | 292 |

TABLE X
HARDWARE USAGE AND PERFORMANCE RESULTS FOR EN BASED ON FIGARO SENSORS, PCA 1, 2 AND KNN

| Hardware resources and performance | Optimization directives | | |
|---|---|---|---|
| | Without Directives | Array Partitioning and Pipelining | AXI Lite Interface |
| BRAM 18K | 4 | 0 | 0 |
| DSP48E | 24 | 133 | 133 |
| FF | 3350 | 35590 | 35626 |
| LUT | 5138 | 47765 | 47805 |
| Max frequency (MHz) | 121 | 97 | 97 |
| Latency (clock cycles) | 5338 | 214 | 214 |

paper. The platform is made of two main parts, the sensing part and the processing part. The sensing part takes the form of a low power temperature sensor and an array of $SnO_2$ gas sensors integrated in a semi-passive RFID tag based on EPC Gen2 standard. The processing part takes the form of a heterogeneous and reconfigurable platform which is the Xilinx Zynq SoC. Various pattern recognition algorithms including PCA, LDA, DT and KNN are implemented on this platform for hardware acceleration and to perform gas identification in real-time. Finally, the heterogeneous hardware/software co-design solution to implement PCA, LDA, DT and KNN on the Zynq SoC as well as the integration of temperature and gas sensors in an RFID tag show promising results in terms of resources usage, power consumption and processing time. It is worth mentioning that the best solution in terms of the classifier to use or the choice of the number of principal components as well the hardware directives will depend on the final application and resources availability. The best solution is the trade-off between the best accuracy, the processing time and the resources available on the hardware. Someone may choose the best accuracy scenario with the fastest implementation for critical and vital applications while compromising on the accuracy and speed is possible for other applications to be able to save on hardware resources and power consumption.

## ACKNOWLEDGMENT

This paper was made possible by National Priorities Research Program (NPRP) grant No. 5-080-2-028 from the Qatar

National Research Fund (a member of Qatar Foundation). The statements made herein are solely the responsibility of the authors.

## REFERENCES


[1] H. E. Matbouly, K. Zannas, Y. Duroc, and S. Tedjini, "Analysis and assessments of time delay constrains for passive rfid tag-sensor communication link: Application for rotation speed sensing," *IEEE Sensors Journal*, vol. 17, no. 7, pp. 2174–2181, April 2017.

[2] A. E. Abdulhadi and T. A. Denidni, "Self-powered multi-port uhf rfid tag-based-sensor," *IEEE Journal of Radio Frequency Identification*, vol. PP, no. 99, pp. 1–1, 2017.

[3] B. Wang, M. K. Law, A. Bermak, and H. C. Luong, "A passive rfid tag embedded temperature sensor with improved process spreads immunity for a $-30°$c to $60°$c sensing range," *IEEE Transactions on Circuits and Systems I: Regular Papers*, vol. 61, no. 2, pp. 337–346, Feb 2014.

[4] A. Vena, E. Perret, D. Kaddour, and T. Baron, "Toward a reliable chipless rfid humidity sensor tag based on silicon nanowires," *IEEE Transactions on Microwave Theory and Techniques*, vol. 64, no. 9, pp. 2977–2985, Sept 2016.

[5] M. R. G. Karkani, M. Kamarei, and A. F. Ahmady, "A low-power smart temperature sensor for passive uhf rfid tags and sensor nets," in *2016 8th International Symposium on Telecommunications (IST)*, Sept 2016, pp. 12–17.

[6] X. Song, G. Wang, and Y. He, "Design of the high-sensitivity rfid sensor tag with moea/d-de," in *2016 International Symposium on Antennas and Propagation (ISAP)*, Oct 2016, pp. 950–951.

[7] M. Zgaren, S. Mohamad, A. Amira, and M. Sawan, "Epc gen-2 uhf rfid tags with low-power cmos temperature sensor suitable for gas applications," in *2016 14th IEEE International New Circuits and Systems Conference (NEWCAS)*, June 2016, pp. 1–4.

[8] ams AG, "Epc class 3 sensory tag chip - for automatic data logging - sl900a data sheet," https://ams.com, 2016, [Online; accessed 30-November-2016].

[9] G. Miskovic, M. V. Nikolic, M. D. Lukovic, Z. Z. Vasiljevic, J. Nicolics, and O. S. Aleksic, "Pseudobrookite thick films for potential application as low-temperature sensitive material in no gas sensors," in *2017 40th International Spring Seminar on Electronics Technology (ISSE)*, May 2017, pp. 1–6.

[10] Y. Liu, H. Liu, T. Hayasaka, Y. Cui, J. Yu, Y. Kubota, X. Li, K. Hu, V. Dasika, L. Nguyen, and L. Lin, "A phase sensitive measurement technique for boosted response speed of graphene fet gas sensor," in *2017 IEEE 67th Electronic Components and Technology Conference (ECTC)*, May 2017, pp. 943–948.

[11] L. Zhang and P. Deng, "Abnormal odor detection in electronic nose via self-expression inspired extreme learning machine," *IEEE Transactions on Systems, Man, and Cybernetics: Systems*, vol. PP, no. 99, pp. 1–11, 2017.

[12] D. Ahmadou, R. Laref, E. Losson, and M. Siadat, "Reduction of drift impact in gas sensor response to improve quantitative odor analysis," in *2017 IEEE International Conference on Industrial Technology (ICIT)*, March 2017, pp. 928–933.

[13] C. Occhiuzzi, A. Rida, G. Marrocco, and M. Tentzeris, "Rfid passive gas sensor integrating carbon nanotubes," *IEEE Transactions on Microwave Theory and Techniques*, vol. 59, no. 10, pp. 2674–2684, 2011.

[14] L. Yang, R. Zhang, D. Staiculescu, C. Wong, and M. M. Tentzeris, "A novel conformal rfid-enabled module utilizing inkjet-printed antennas and carbon nanotubes for gas-detection applications," *IEEE Antennas and Wireless Propagation Letters*, vol. 8, pp. 653–656, 2009.

[15] J. Yin, J. Yi, M. K. Law, Y. Ling, M. C. Lee, K. P. Ng, B. Gao, H. C. Luong, A. Bermak, and M. Chan, "A system-on-chip epc gen-2 passive uhf rfid tag with embedded temperature sensor," *IEEE Journal of Solid-State Circuits*, vol. 45, no. 11, pp. 2404–2420, 2010.

[16] M. Shi, A. Bermak, S. Chandrasekaran, A. Amira, and S. Brahim-Belhouari, "A committee machine gas identification system based on dynamically reconfigurable fpga," *IEEE Sensors Journal*, vol. 8, no. 4, pp. 403–414, 2008.

[17] F. Benrekia, M. Attari, and M. Bouhedda, "Gas sensors characterization and multilayer perceptron (mlp) hardware implementation for gas identification using a field programmable gate array (fpga)," *Sensors*, vol. 13, no. 3, pp. 2967–2985, 2013.

[18] K. T. Ng, B. Guo, A. Bermak, D. Martinez, and F. Boussaid, "Characterization of a logarithmic spike timing encoding scheme for a $4\times$ 4 tin oxide gas sensor array," in *Sensors, 2009 IEEE*. IEEE, 2009, pp. 731–734.

[19] K. Ting Ng, B. Guo, D. Martinez, F. Boussaid, and A. Bermak, "A $4\times$ 4 tin oxide gas sensor array based on spike sequence matching," in *2008 2nd International Conference on Signals, Circuits and Systems, SCS 2008*, 2008.

[20] Q. Li and A. Bermak, "A low-power hardware-friendly binary decision tree classifier for gas identification," *Journal of Low Power Electronics and Applications*, vol. 1, no. 1, pp. 45–58, 2011.

[21] A. B. Far, F. Flitti, B. Guo, and A. Bermak, "A bio-inspired pattern recognition system for tin-oxide gas sensor applications," *IEEE Sensors Journal*, vol. 9, no. 6, pp. 713–722, 2009.

[22] E. Kim, S. Lee, J. H. Kim, C. Kim, Y. T. Byun, H. S. Kim, and T. Lee, "Pattern recognition for selective odor detection with gas sensor arrays," *Sensors*, vol. 12, no. 12, pp. 16 262–16 273, 2012.

[23] S. B. Belhouari, A. Bermak, G. Wei, and P. Chan, "Gas identification algorithms for microelectronic gas sensor," in *Instrumentation and Measurement Technology Conference, 2004. IMTC 04. Proceedings of the 21st IEEE*, vol. 1. IEEE, 2004, pp. 584–587.

[24] M. Hassan and A. Bermak, "Robust bayesian inference for gas identification in electronic nose applications by using random matrix theory," *IEEE Sensors Journal*, vol. 16, no. 7, pp. 2036–2045, 2016.

[25] M. Hassan, S. B. Belhaouari, and A. Bermak, "Probabilistic rank score coding: A robust rank-order based classifier for electronic nose applications," *IEEE Sensors Journal*, vol. 15, no. 7, pp. 3934–3946, 2015.

[26] M. Hassan and A. Bermak, "Biologically inspired feature rank codes for hardware friendly gas identification with the array of gas sensors," *IEEE Sensors Journal*, vol. 16, no. 14, pp. 5776–5784, 2016.

[27] S. Brahim-Belhaouari, M. Hassan, N. Walter, and A. Bermak, "Advanced statistical metrics for gas identification system with quantification feedback," *IEEE Sensors Journal*, vol. 15, no. 3, pp. 1705–1715, 2015.

[28] M. Hassan and A. Bermak, "Gas classification using binary decision tree classifier," in *2014 IEEE International Symposium on Circuits and Systems (ISCAS)*. IEEE, 2014, pp. 2579–2582.

[29] Figaro-Inc, "Figaro Sensors," http://www.figarosensor.com/, 2015, [Online; accessed 30-September-2016].

[30] B. Guo, A. Bermak, P. C. Chan, and G.-Z. Yan, "An integrated surface micromachined convex microhotplate structure for tin oxide gas sensor array," *Sensors Journal, IEEE*, vol. 7, no. 12, pp. 1720–1726, 2007.

[31] Xilinx-Inc, "Zc702 evaluation board for the zynq-7000 xc7z020 all programmable soc: User guide. ug850, v1.5," http://www.xilinx.com, 2015, [Online; accessed 30-September-2016].

[32] Xilinx-Inc, "Zynq-7000 all programmable soc: Technical reference manual. ug585, v1.11," http://www.xilinx.com, 2016, [Online; accessed 30-September-2016].

[33] Xilinx-Inc, "Zynq-7000 all programmable soc: Overview. ds190, v1.10," http://www.xilinx.com, 2016, [Online; accessed 30-September-2016].

[34] Xilinx-Inc, "Vivado design suite user guide: High-level synthesis. ug902, v2016.3," http://www.xilinx.com, 2013, [Online; accessed 30-October-2016].

[35] H. Djelouat, A. Ait Si Ali, A. Amira, and F. Bensaali, "An interactive software tool for gas identification," *Journal of Natural Gas Science and Engineering*, 2017.

[36] A. Ait Si Ali, H. Djelouat, A. Amira, F. Bensaali, M. Benammar, and A. Bermak, "Electronic nose system on the zynq soc platform," *Microprocessors and Microsystems*, vol. 53, pp. 145–156, 2017.

[37] M. A. Akbar, A. Ait Si Ali, A. Amira, F. Bensaali, M. Benammar, M. Hassan, and A. Bermak, "An empirical study for pca-and lda-based feature reduction for gas identification," *IEEE Sensors Journal*, vol. 16, no. 14, pp. 5734–5746, 2016.

[38] H. Djelouat, A. Ait Si Ali, A. Amira, and F. Bensaali, "Compressive sensing based electronic nose platform," *Digital Signal Processing*, vol. 60, pp. 350–359, 2017.